V European Conference on Computational Fluid Dynamics
ECCOMAS CFD 2010
J. C. F. Pereira and A. Sequeira (Eds)
Lisbon, Portugal,14-17 June 2010

IMPLICIT LARGE-EDDY SIMULATION OF NOISE RADIATED BY A SUBSONIC JET AT HIGH REYNOLDS NUMBER

Carlos A. S. Moser*, Jorge H. Silvestrini† and Marcello A. F. Medeiros††

*Dept. Aeronautical Engineering - University of São Paulo,
São Carlos, SP - Brazil - CEP 13560-970
carlos.moser@yahoo.com.br
†Dept. Mechanical and Mechatronics Engineering - PUCRS,
Porto Alegre, RS - Brazil - CEP 90619-900
jorgehs@pucrs.br
††Dept. Aeronautical Engineering - University of São Paulo,
São Carlos, SP - Brazil - CEP 13560-970
marcello@sc.usp.br

Key words: Computational Aeroacoustics, Implicit LES, Subsonic Jet, Noise Radiation

Abstract. *A methodology to perform the implicit large-eddy simulation (LES) of the jet noise radiated at high Reynolds number was developed. Unlike eddy-viscosity type models, this approach assumes that the subgrid model may be determined by the structure of the resolved flow and, therefore, does not require any additional subgrid-scale stress or heat flux terms. High-order compact schemes were used for the spatial discretization and a fourth-order Runge-Kutta method was used for the time integration. The high-frequency content of the smallest unresolved subgrid scales was removed by the application of high-order filtering, while the effect of these scales on the largest filtered scales was reconstructed by an approximate deconvolution model. The non-conservative form of the compressible Navier-Stokes equations was used to compute the flow solution in the physical domain. While a characteristic-based formulation of the flow equations combined with a conceptual model based on the characteristic analysis were employed to prescribe boundary conditions and buffer zone treatments. By this modeling approach outgoing waves exit the domain without generating high-frequency spurious wave reflections, which can contaminate the acoustic field solution. Implicit LES were carried out to investigate the aerodynamic noise radiated by the well-known test case of a Mach* 0.9 *jet at Reynolds number* 6.5×10^4 *. Effects of grid resolution on the jet shear-layer characteristics, such as the jet inlet shear-layer momentum thickness, were analysed. In the ongoing work, a parallel high-order flow solver is being implemented to perform implicit LES of the noise radiated by 3D subsonic round jets at high Reynolds number.*

1 INTRODUCTION

Noise radiation from an extensive region of unsteady hydrodynamics was firstly investigated by Colonius et al.[12] by performing direct numerical simulation (DNS) of the sound generated by a two-dimensional mixing layer. The presence of flow-acoustic interactions in the acoustic field was found to be very sensitive to small changes in the computed flow-noise source. Mitchell et al.[27] performed the DNS for both the flow and the sound radiated from subsonic and supersonic axisymmetric 2D jets. The predicted sound was found to agree with predictions of Lighthill's acoustic analogy. Freund et al.[14] reported the DNS of a turbulent jet at Mach number 1.92. As the flow was nearly isothermal, the principal noise radiation mechanism was Mach waves generated by supersonically advecting flow structures. Bogey and Bailly[8] computed by LES the sound field of a Mach 0.9 jet at Reynolds number 6.5×10^4 with the Smagorinsky model. Based on the unsteady flow results obtained, they directly computed the aerodynamic noise. The mean flow and turbulence intensities, as well as sound directivity and sound levels, were found to be in good agreement with experimental data. Bodony and Lele[1] conducted a systematic investigation of LES's predictive capability for jet noise at the Reynolds number range from 1.3×10^4 to 3.36×10^5. Noise predictions for the unheated and heated jets were found to be in agreement with experimental data[35]. Bogey and Bailly[7] showed that inflow conditions, particularly the spatial structure of inflow disturbances, can significantly impact the development of jet flows and the radiated sound predicted by compressible LES at high Reynolds numbers. Some attempts on round jets have been made by Choi et al.[10] and Boersma and Lele[2]. Nevertheless, except for some recent studies of Bogey and Bailly[4,5,7] and Bodony and Lele[1], the highest Reynolds numbers reached in the LES simulations are still far bellow those of practical interest.

The main goal of the present work is to develop and validate an implicit LES method based on approximate deconvolution[33] and high-order filtering[36] by the analysis of grid resolution effects on the jet shear layer characteristics. In order to satisfy strict requirements of aeroacoustic computations at high Reynolds number, such as the large difference of scales between the flow and the acoustic field, high-order compact schemes[22] were used for spatial discretization and a fourth-order Runge-Kutta method was employed for time integration. The non-conservative form of the compressible Navier-Stokes equations was used to compute the flow solution in the physical domain. While a characteristic-based formulation[32] was used to prescribe boundary conditions and the buffer zone. The wave modal structure provided by this formulation allows us to define non-reflecting boundary conditions and buffer zone treatments especially adapted for aeroacoustic computations. Non-reflecting boundary conditions were specified to let outgoing disturbances exit the computational boundaries without producing spurious wave reflections. Downstream of the physical domain, a buffer zone[11] was attached to damp outgoing disturbances before they interact with the outflow boundary. Additionally, grid stretching was applied in the buffer zone to help to dissipate large-scale disturbances of the jet flowfield.

2 LARGE-EDDY SIMULATION METHODS

In the last few years, LES has achieved significant progress due to advances in computational power, numerical algorithms and subgrid-scale models. LES has been applied to a wide variety of turbulent flows, ranging from problems of scientific interest to those with engineering applications. This trend has been motivated by the need to provide a more realistic characterization of complex unsteady flows encountered in areas such as flow control, aeroacoustics and fluid/structure interaction. Nevertheless, the vast majority of LES research has been devoted to incompressible flows; while compressible flow applications have only recently gained some attention, due to the increased complexity introduced by the need to model the energy equation[30,38].

2.1 Subgrid Eddy-Viscosity Type Models

LES methods for compressible flows have ranged from using the inherently limited Smagorinsky eddy-viscosity type models, to more sophisticated and accurate dynamic models. The Smagorinsky-type models exhibit two major drawbacks. They ignore turbulence anisotropy and use a local balance assumption between the subgrid scale turbulence kinetic energy production and its dissipation. Furthermore, they predict non-vanishing subgrid eddy viscosity in regions where the flow is laminar. The dynamic procedures[18,24] for computing the model coefficient from the resolved velocity field, which require no adjustable constant, overcome these shortcomings. However, the numerical stabilization become complicated when the dynamic model is applied to flow configurations in which there are inhomogeneous directions. Vreman[37] developed a subgrid eddy-viscosity type model especially suitable for laminar shear flows, since it vanishes subgrid dissipation in laminar regions and does not require any averaging or clipping procedure for numerical stabilization. Park et al.[29] proposed a dynamic procedure for determining the model coefficient utilizing the global equilibrium between the subgrid and viscous dissipation. In this approach, the model coefficient is globally constant in space but varies in time, and it still garantees zero eddy viscosity in the laminar flow regions.

In traditional LES methods, the equations are obtained by spatial filtering of the flow variables. Ideally, for incompressible flows the filtering of the Navier-Stokes equations generates a closure problem in the form of an unknown residual subgrid-scale stress tensor:

$$\tau_{i,j} = \overline{u_i u}_j - \bar{u}_i \bar{u}_j \tag{1}$$

It should be emphasized, however, that the filtering equations are not closed because of the presence of the nonlinear term $\overline{u_i u}_j$, since the subgrid-scale stress tensor stems from a closure problem introduced by the spatial filtering operation and not from the discretization's inability to represent the small scales in the flow. As a result, the subgrid-scale stress tensor strongly depends on the assumed filter shape, which causes a subgrid-scale model to be inherently filter dependent. Hence, depending on the choice of the filter, the corresponding model should satisfy very different requirements in terms of large-scale dynamics and kinetic energy budget.

2.2 Implicit LES Approach

An alternative approach to subgrid eddy-viscosity type models is the use of high-order spatial filters to implictly model the energy content present in the poorly resolved smallest scales of the flow. This aproach does not require any additional subgrid scale stress or heat flux terms in the flow governing equations. Although the filter is applied explicitly to the evolving solution, this approach is referred as implicit LES, since the application of the spatial filter is a fundamental component to mantain stability by removing high-frequency spurious numerical oscillations. The basis of the implicit LES approach is that the numerical truncation error associated with the discretization has similar form or action to the subgrid model. Such approach falls into the class of structural models, since there is no assumed form of the nature of the subgrid flow. The subgrid model is entirely determined by the structure of the resolved flow[31]. Nevertheless, even with the recently increase of interest in implicit LES, there is not a consensus on the appropriate form of the discretization error, since it is assumed that the numerics provide sufficient modeling of the subgrid terms to allow correct dissipation of turbulent kinetic energy.

The analysis of the impact of spatial discretization errors on implicit LES establishes the need of high-order spatial filtering[16]. The high order filtering of Navier-Stokes equations should provides dissipation at the higher modified wave numbers only, where the spatial discretization already exhibits significant dispersion errors, and enforce numerical stability on nonuniform grids. The filtering also should allow to eliminate numerical instabilities arising from poor grid quality, unresolved scales, or boundary conditions, which left to grow can potentially corrupt the flow solution. The filtering operation is defined by Leonard [23] in the physical space as

$$\bar{f}(x) = \int_{\Omega} f(x')G(x, x'; \delta)dx' \tag{2}$$

where Ω is the entire domain, G is the filter kernel and δ is the filter width associated to the smallest scale retained by the filtering operation. Thus, $\bar{f}$ defines the size and structure of the small scales.

In principle, to mantain acceptable numerical acurracy and proper resolution of low wavenumbers, the filter accuracy should be equal or greater than the corresponding accuracy of the spatial discretization scheme. Thus, the flow variables were filtered in every spatial direction at the final stage of each time step with sixth-order implicit filters[36]. Sixth-order compact finite difference schemes[22] were employed for the spatial discretization and the fourth-order Runge-Kutta method was used for the temporal integration.

At the interior grid points $i = 4, ..., N-3$, the implicit filtering approach is defined as follows

$$\alpha_f \bar{f}_{i-1} + \bar{f}_i + \alpha_f \bar{f}_{i+1} = \sum_{n=1}^{4} \frac{a_n}{2}(f_{i-n+1} + f_{i+n-1}) \tag{3}$$

The coefficients a_n are derived in terms of the filtering parameter α_f by Taylor and Fourier series analysis[15;16]

$$a_1 = +\tfrac{11}{16} + \tfrac{5}{8}\alpha_f, \quad a_2 = +\tfrac{15}{32} + \tfrac{17}{16}\alpha_f,$$
$$a_3 = -\tfrac{3}{16} + \tfrac{3}{8}\alpha_f, \quad a_4 = +\tfrac{1}{32} + \tfrac{1}{16}\alpha_f,$$

where α_f must satisfy the inequality $-0.5 \leq \alpha_f \leq 0.5$. Filters less dissipative are obtained with higher values of α_f within the given range, and for $\alpha_f = 0.5$ there is no filtering effect. By contrast, the explicit filter ($\alpha_f = 0$) display significant degradation of the spectral frequency response. Here the filter parameter was fixed as $\alpha_f = 0.40$.

As equation (3) has a right-hand side stencil of seven points, obviously it can not be employed near the boundaries of the computational domain. Thus, the following implicit filter is used at the grid points $i = 2$ and 3:

$$\alpha_f \bar{f}_{i-1} + \bar{f}_i + \alpha_f \bar{f}_{i+1} = \sum_{n=1}^{7} a_{n,i} f_n \tag{4}$$

For $i = 2$:

$$a_{1,2} = +\tfrac{1}{64} + \tfrac{31}{32}\alpha_f, \quad a_{2,2} = +\tfrac{29}{32} + \tfrac{3}{16}\alpha_f,$$
$$a_{3,2} = +\tfrac{15}{64} + \tfrac{17}{32}\alpha_f, \quad a_{4,2} = -\tfrac{5}{16} + \tfrac{5}{8}\alpha_f,$$
$$a_{5,2} = +\tfrac{15}{64} - \tfrac{15}{32}\alpha_f, \quad a_{6,2} = -\tfrac{3}{32} + \tfrac{3}{16}\alpha_f,$$
$$a_{7,2} = +\tfrac{1}{64} - \tfrac{1}{32}\alpha_f.$$

For $i = 3$:

$$a_{1,3} = -\tfrac{1}{64} + \tfrac{1}{32}\alpha_f, \quad a_{2,3} = +\tfrac{3}{32} + \tfrac{13}{16}\alpha_f,$$
$$a_{3,3} = +\tfrac{49}{64} + \tfrac{15}{32}\alpha_f, \quad a_{4,3} = -\tfrac{5}{16} + \tfrac{5}{8}\alpha_f,$$
$$a_{5,3} = -\tfrac{15}{64} + \tfrac{15}{32}\alpha_f, \quad a_{6,3} = +\tfrac{3}{32} - \tfrac{3}{16}\alpha_f,$$
$$a_{7,3} = -\tfrac{1}{64} + \tfrac{1}{32}\alpha_f.$$

Analogously, at the grid points $i = N - 2$ and $N - 1$:

$$\alpha_f \bar{f}_{i-1} + \bar{f}_i + \alpha_f \bar{f}_{i+1} = \sum_{n=1}^{7} a_{n,N-i+1} f_{N-n+1} \tag{5}$$

While at the boundary points $i = 1$ and N, the flow variables were kept without application of any filtering operation.

2.3 Approximate Deconvolution Model

The implicit LES approach re-interpreted by Mathews et al. [25] in the context of an approximate deconvolution model[33] was used in present study to compute the filtered solution variable $\bar{u}$, by the following filtering operation

$$\bar{u} = G * u = \int G(x - x')u(x')dx' \tag{6}$$

where G is the filter transfer function. If G has an inverse Q, an approximation of the unfiltered variable u, denoted by u^*, may be obtained by deconvolution of the filtered

variable $\bar{u}$ as

$$u^* = Q * \bar{u} \tag{7}$$

where the inverse filter transfer function Q may be obtained by a truncated power series expansion

$$Q_N = \sum_{\nu=0}^{N} (I - G)^{\nu} \tag{8}$$

where I is the identity matrix and $N = 1, 2, 3, ...$ the number of filtering steps. The family of inverse filter transfer functions, Q_N, is based on the iterative deconvolution method of Galdi [17]. High-order approximations u^* from the unfiltered variable u, can be derived by sucessive filtering operations applied to the filtered quantities

$$u^* = \bar{u} + (I - G) * \bar{u} + (I - G) * ((I - G) * \bar{u}) + ... \tag{9}$$

In smooth regions of the flow, these filters have strong stability properties and high consistency error $O(\delta^{2N+2})$, where δ is the filter width. As reported by Stolz et al. [34], the truncation order of the Eq. (9) determines the level of deconvolution. Here we choose the third level quadratic extrapolation: $u^* \approx Q_2\bar{u} := 3\bar{u} - 3\bar{\bar{u}} + \bar{\bar{\bar{u}}}$, since it affords a sufficiently high-order consistency error $O(\delta^5)$.

3 FLOW CONFIGURATION

3.1 Inflow Boundary Conditions

In the implicit LES of the jet, the inflow boundary conditions have been modeled by imposing the following hyperbolic-tangent mean velocity profile

$$u(r) = \frac{U_j}{2}\left(1 + \tanh\left(\frac{r_o - r}{2\delta_\theta}\right)\right) \tag{10}$$

where U_j is the jet inlet centerline velocity, r_o is the jet radius and δ_θ is the inlet shear-layer momentum thickness. The jet inlet velocities are normalized by the sound speed in the ambient medium c_o and the Reynolds number of the flow is

$$Re_D = \frac{U_j \times D}{\nu} \tag{11}$$

where $D = 2r_o$ is the jet width and ν the kinematic viscosity.

3.2 Near-Inflow Periodic or Random Excitations

In order to startup earlier the turbulent mixing process in the jet shear layer, a low-amplitude excitation of incompressible nature, i.e. with zero divergence[6] is added to the velocity field, just downstream of the inflow boundary. The axisymmetric structure of this

excitation has the form of a vortex ring of radius $y_o = r_o$, with streamwise and transverse velocities

$$U_{x_o} = 2\,\frac{y_o}{y}\,\frac{y-y_o}{\Delta_o}\,\mathrm{Exp}\left(-\mathrm{Ln}\,2\,\left(\frac{\Delta_{x,y}}{\Delta_o}\right)^2\right)$$
$$U_{y_o} = 2\,\frac{y_o}{y}\,\frac{x-x_o}{\Delta_o}\,\mathrm{Exp}\left(-\mathrm{Ln}\,2\,\left(\frac{\Delta_{x,y}}{\Delta_o}\right)^2\right) \tag{12}$$

where $y \neq 0$ and $\Delta^2_{x,y} = (x-x_o)^2 + (y-y_o)^2$. Δ_o is the minimum grid spacing in the shear layer and x_o is the streamwise location of the center of the excitation, chosen as $x_o = 0.80y_o$. The velocity fluctuations given by Eq.(12) are then added onto the local velocity components

$$u_x = u_x + U_{x_o}U_j\sum_{i=0}^{n}\alpha_n\epsilon_n\mathrm{Cos}(\theta_n+\phi_n)$$
$$u_y = u_y + U_{y_o}U_j\sum_{i=0}^{n}\alpha_n\epsilon_n\mathrm{Cos}(\theta_n+\phi_n) \tag{13}$$

where α_n, ϕ_n and θ_n are, respectively, the amplitude, phase and azimuthal angle of each one of the $n+1$ modes of excitation. The parameters for random excitations are $\theta_n = n\theta$, $\epsilon_n = [-1,1]$, $\phi_n = [0,\pi]$ and $\alpha_n = 2.5\times10^{-4}$, where n was set to 9. While for periodic excitations $\epsilon_n = 1$ and $\theta_n = 2\pi f_n t$, where f_n are the excitation frequencies and t is the time step, with n set to 1.

In the jet shear layer, instabilities are governed by two different modes associated with two different characteristic length scales: the inlet shear-layer momentum thickness δ_θ and the jet width D. The first mode is the fundamental frequency f_o of the velocity fluctuations. This mode is observed in the neighborhood of the jet inlet and is responsible by the exponential growth of shear layer instabilities. The linear instability theory[26] predicts that the strongest amplification rate of perturbations for the hyperbolic-tangent velocity profile given by Eq. (10) is observed for

$$fo = 0.017\frac{U_j}{\delta_\theta} \tag{14}$$

The second mode, known as the first sub-harmonic $f_1 = f_o/2$, corresponds to the frequency of the vortex pairing process. In the current calculations this mode also characterizes the frequency of the velocity fluctuations that occurs in the jet potential core, with amplitudes fixed as $\alpha_o = 2.5\times10^{-4}$ and $\alpha_1 = \alpha_o/3$, and phases as $\phi_o = 0$ and $\phi_1 = \pi/2$.

3.3 Buffer Zone

Similarly to Colonius et al. [11], a buffer zone is attached downstream of the physical domain to damp large-scale vortical structures originated by the turbulent jet flow. These structures are effectively dissipated in the buffer zone, before they interact with the outflow boundary, by adding artificial damping terms to the flow governing equations

$$\left.\frac{\partial \mathbf{Q}}{\partial t}\right|_{dp} = \frac{\partial \mathbf{Q}}{\partial t} - \sigma_{dp}\mathbf{Q}' \tag{15}$$

$\mathbf{Q}$ is the solution vector $[u, p]$ and σ_{dp} is a damping function defined as

$$\sigma_{dp}(r) = \frac{1}{4}\left(1 + \tanh\left(a_o \frac{r - 2r_o}{2\delta_\theta}\right)\right) \tag{16}$$

with $r^2 = x^2 + y^2$ and $a_o = 0.575$.
The disturbance $\mathbf{Q}'$ in the Eqs. (15) is computed at every time step t as follows

$$\mathbf{Q}'_{(t)} = \mathbf{Q}_{(t)} - \left(\alpha \bar{\mathbf{Q}}_{(t-1)} + (1 - \alpha)\mathbf{Q}_{(t)}\right) \tag{17}$$

where $\bar{\mathbf{Q}}_{(t-1)}$ is the time-average solution computed in the previous time step and $\alpha = 0.90$. Additionally, was applied in the buffer zone the grid stretching to help to dissipate the large-scale disturbances of the jet flowfield.

3.4 Non-Reflecting Boundary Conditions

As in aeroacoustic computations the domain must be large enough to allow wave propagation in the far-field, the deviations from the flow velocity fluctuations are likely to be small owing solely to acoustic fluctuations. Therefore, far-field non-reflecting boundary conditions may be obtained by simply setting to zero the incoming waves at the outflow and lateral boundaries. Reflections of spurious waves generated by the excitation at the inflow boundary were minimized by the application of a near-inflow absorbing zone[28].

4 RESULTS

In this work, the Reynolds number was set to 6.5×10^4 and the Mach number to 0.9. The choice of this Mach number may be justified by the considerable amount of numerical and experimental studies at similar flow conditions. The Reynolds number adopted is an intermediate value between jets obtained by DNS ($Re_D < 10^3$) and experimental jets ($Re_D > 10^5$). The inlet momentum thickness was chosen as $\delta_\theta = 0.05 r_o$, which is large enough to afford the development of turbulent structures in the jet shear layer before the end of the potential core. The preliminary tests for evaluation and validation of the present implicit LES approach were performed in a two-dimensional flow configuration to reduce

the inherently high computational cost of 3D computations. The mesh was discretized in Cartesian coordinates with 255×225 grid points in a computational domain which extends to $50r_o$ in the streamwise direction and from $-25r_o$ to $25r_o$ in the transverse direction. As the velocity gradients are more pronounced in the jet shear layer, the mesh was more refined in this region, with an uniform grid spacing of $\Delta y = r_o/32$. Outside the shear layer the grid was gradually stretched up to an uniform grid spacing of $0.602r_o$ in the acoustic field. In the streamwise direction, the grid discretization was relatively coarser, with an uniform grid spacing of $0.071r_o$ from the jet inlet up to the end of the potential core. The grid was gradually stretched downstream of the potential core up to a maximum grid spacing of $1.402r_o$ at the outflow boundary.

4.1 Grid Resolution Effects on the Jet Shear Layer Characteristics

The development of turbulence by the jet is very sensitive to inflow conditions characterizing the jet shear layer evolution[9,19]. As reported by several studies of jets, small variations on the inflow conditions can significantly change the jet shear layer characteristics. Kim and Choi [21] observed that inflow conditions effects on jet characteristics, as the momentum thickness and the Reynolds number, substantially depend on the accurate resolution of the jet shear layer. In the LES of a 3D round jet [3] was employed 26 grid points to discretize the jet half-width. However, the LES of round jets using explicit selective/high-order filtering [7], the jet radius was discretized in a Cartesian grid with 15 points. Therefore, understanding grid resolution effects on the jet characteristics may be critical for predicting the jet flow dynamics.

Effect of grid resolution were investigated by forcing the near-inlet shear layer region, just downstream of the inflow boundary, with low-amplitude periodic and random excitations. The inverse of the jet mean centerline velocity, U_j, normalized by the jet inlet mean centerline velocity, U_c is represented in Fig.1 for different grid resolutions. To accurately resolve the large gradients of velocity in the shear layer, the grid points were gradually clustered, by locally decreasing the grid spacing from $\Delta y = r_o/18$ to $r_o/36$. When the grid spacing was decreased from $\Delta y = r_o/32$ to $r_o/36$ in the jet shear layer, it may be observed the convergence, since the curves U_j/U_c tend to be superposed. As the initial shear layer evolution is laminar for the current jet inflow conditions ($Re_D = 6.5 \times 10^4$ and $\delta_\theta = 0.05r_o$), it appears that the jet mean centerline velocity should be constant in the whole jet potential core. However, small fluctuations on the jet mean centerline velocity were detected within the jet potential core, for $5 \leq x/r_o \leq 9$. It is important to notice, that this behavior within the potential core has already been observed experimentally [20] and numerically [7]. In the far downstream region, as expected, we see that the inverse of the jet centerline velocity decaying rate presents linear growth for both periodic and random excitations. Nevertheless, when the jet near-inlet shear layer region was periodically excited, the potential core breaks up earlier and the inverse of the velocity decaying rate presents smaller growth in the far downstream region.

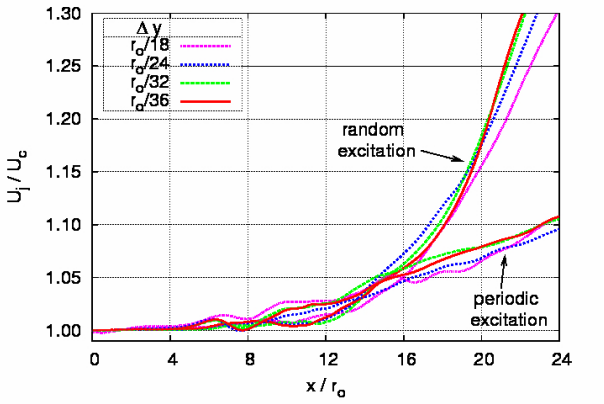

Figure 1: Representation of the inverse of the jet mean centerline velocity, U_c, for different grid resolutions in the jet shear layer, excited with random and periodic excitations.

In figures 2(a)-(d) were evaluated, for different grid resolutions in the jet shear layer, the instantaneous of vorticity field, $\omega_{xy} = \partial v/\partial x - \partial u/\partial y$, of a periodically excited jet. As show Figs.2(a) and (b), for about $x = 3r_o$, the initial shear-layer tickness was strongly affected by the coarser resolutions in the jet shear layer. The coarser meshes introduce an upstream effect on the initial shear layer evolution, such that the initial shear-layer tickness is affected by feedback effects from the downstream development of the large-scale vortices[13]. Nevertheless, when finer meshs were used in Figs.2(c) and (d), the initial shear layer evolution was almost unaffected by feedback effects. Thus, for the present shear-layer tickness, $\delta_\theta = 0.05r_o$, it was required at most the grid spacing of $\Delta y = r_o/32$ in the jet shear layer to achieve accurate predictions of the jet flow dynamics.

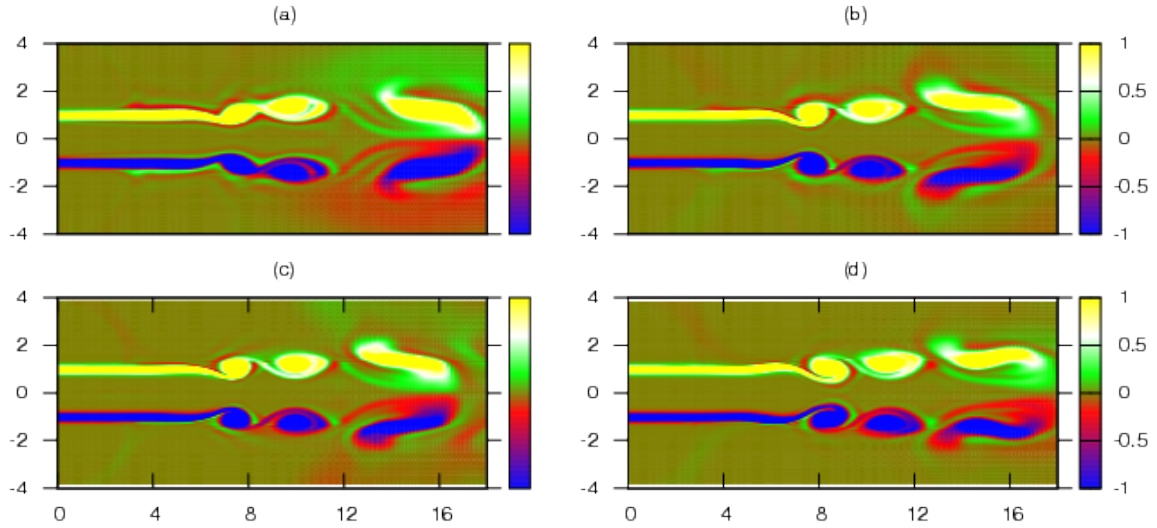

Figure 2: Representation of the vorticity field, ω_{xy}, for the grid resolutions: (a) $\Delta y = r_o/18$; (b) $r_o/24$; (c) $r_o/32$ and (d) $r_o/36$ in the jet shear layer. Physical domain for $0 \leq x/r_o \leq 18$ and $-4 \leq y/r_o \leq 4$.

4.2 Aerodynamic Noise Generation by the Vortex Pairing Proccess

The complet cycle of noise generation by the vortex pairing proccess in the jet shear layer is depicted in Fig.3 by the snapshots of vorticity, ω_{xy}, at four successive instants of time separated by $T_p/4$, where T_p is the period of time. The introduction of a low-amplitude periodic excitation in the near-inlet shear layer region trigger the non-linear growth of Kelvin-Helmholtz instabilities, which rapidly evolve and saturate downstream to form large-scale vortical structures axisymmetrically distributed in the jet shear layer. The evolutive proccess of growth, approximation, interaction, pairing and merging of two consecutive vortical structures in the jet shear layer give rise to the vortex pairing process. The details of vorticity field reveal that the vortex pairing is not responsible for feedback mechanisms on the jet flow dynamics. The vortex pairing proccess occurs at a fixed position around $x = 12r_o$ every period of time $T_p = 1/f_p$ with frequence $f_p = f_o/2$, where f_o is the fundamental frequency of the excitation. The merging of two consecutive vortical structures generates a larger-scale vortex, which is convected downstream by the flow. It should be remarked that the large-scale vortical structures which are originated after the vortex pairing process must be rapidly dissipated in the buffer zone (located after $x = 18r_o$) to avoid the eventual development of other vortex pairings, which may introduce undesirable secondary sound sources in the jet shear layer.

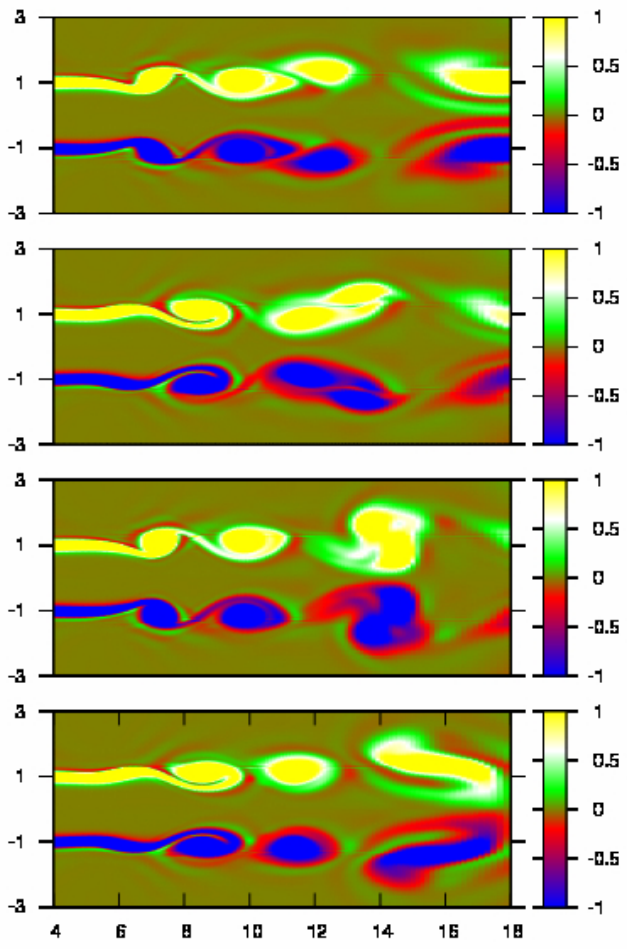

Figure 3: Vortex pairing proccess in the jet shear layer. Snapshots of vorticity, ω_{xy}, represented at four successive instants of time, separated by $T_p/4$. Physical domain for $4 \leq x/r_o \leq 18$ and $-3 \leq y/r_o \leq 3$.

4.3 Acoustic Field Propagation

The acoustic field generated aerodynamically by vortex pairing process described in the previous section is depicted by the dilatation, $\Theta = \nabla.u$, in Fig.4. The complete cycle

of noise propagation is described by the snapshots of dilatation at four sucessive instants of time, separated by $T_p/4$. The acoustic field solution is displayed on the whole computational domain for $0 < x/r_o < 50$ and $-25 < y/r_o < 25$, except on the buffer zone of aerodynamic dissipation, located after $x/r_o = 18$ and for $-4 < y/r_o < 4$. Even with a relatively small width compared to the domain width, the buffer zone is able to efficiently dissipate all aerodynamic instabilities which arise in the near-field mixing region downstream of the vortex pairing location, avoiding the eventual appearance of other secondary vortex pairing sound sources, which can contaminate the original acoustic field solution. It is important to remark that the fully computational domain is represented in Fig.4. This domain does not require any artificial acoustic absorbing region at the outflow boundary and at the far-field boundaries, what considerably simplifies the numerical implementation and reduces the computational cost. The acoustic field propagation and the corresponding vortex pairing proccess in the jet shear layer described above present qualitative agreement with previous results obtained from three-dimensional simulations of axisymmetric round jets[3] at the same Reynolds number and jet inlet momentum thickness.

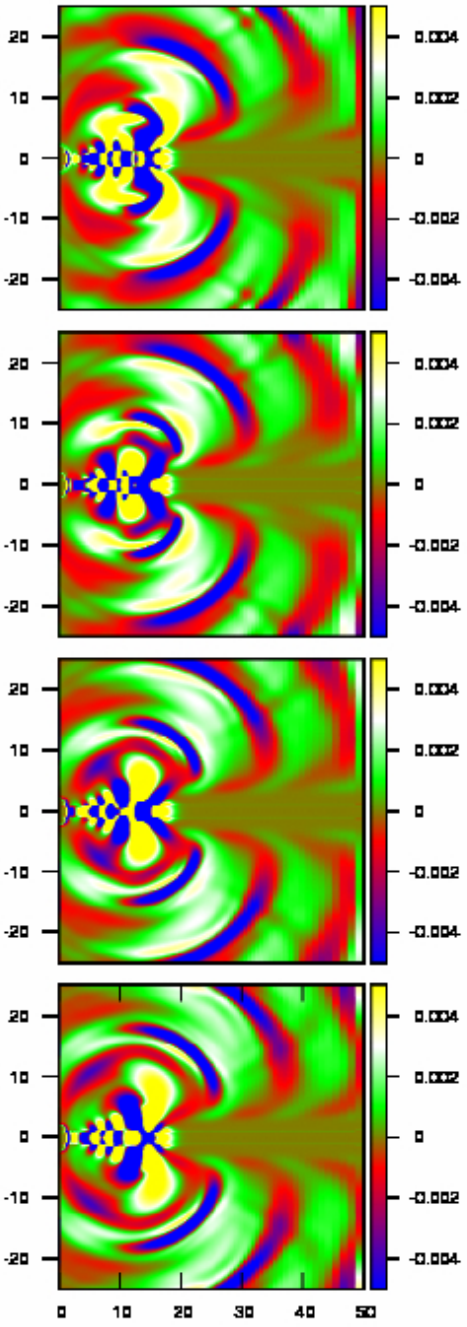

Figure 4: Acoustic field propagation represented by the dilatation, $\Theta = \nabla.u$, at four successive instants of time, separated by $T_p/4$. The computational domain $0 \leq x/r_o \leq 50$ and $-25 \leq y/r_o \leq 25$ includes a buffer zone for $18 \leq x/r_o \leq 50$ and $-4 \leq y/r_o \leq 4$.

4.4 Aerodynamic Flow Noise-Source and Acoustic Field Propagation

The aerodynamic flow noise-source region and the acoustic field propagation are represented in Fig.5 by the vorticity, ω_{xy}, and dilatation, Θ. It is important to remark that both fields were directly computed by the present implicit LES procedure without the need of any modeling approach. It should be noticed in Fig.5 that the acoustic wavefronts propagate

from the region of the aerodynamic field that give rise to the vortex pairing process, which is located at the end of the potential core at around $x/r_o = 12$.

Thus, it was verified that the only dominant noise source in the jet shear layer is the noise radiated from the region where the vortex pairing takes place. The absence of spurious waves near the inflow is due to the incompressible nature[6] of the excitation. It should be noted that the acoustic waves propagate through the far-field boundary without producing any significant spurious wave reflections, because of the application of the nonreflecting boundary condition. The noise radiated on the acoustic field decays to zero for an angle around 80^o, with phase shifting for wider angles of radiation relative to the shear layer axis. This particularly high directive character of sound radiation, especially noticed at high Mach numbers, is attributed to the axisymmetric quadrupolar nature of the sound source, as already observed by LES of three-dimensional jets[8].

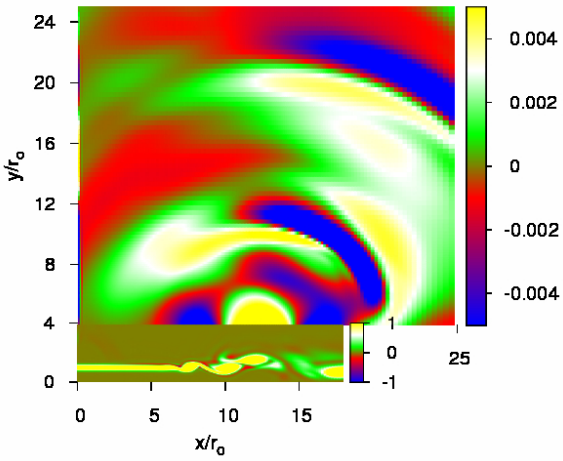

Figure 5: Aerodynamic and acoustic fields represented, respectively, by the vorticity, ω_{xy} and dilatation, Θ. Upper regions of the physical domain, excluding the buffer zone of aerodynamic dissipation located after $x/r_o = 18$.

5 CONCLUDING REMARKS

Preliminary tests were carried out for evaluation and validation of a highly accurate implicit LES approach especially developed for the computation of the aerodynamic noise radiated from a Mach 0.9 cold jet at Reynolds number 6.5×10^4. To startup earlier the turbulent mixing process in the jet shear layer, the near-inlet shear layer region was forced with low-amplitude periodic or random excitations, Effects of grid resolution on the jet shear layer characteristics were investigated for the jet inlet shear layer momentum thickness $\delta_\theta = 0.05 r_o$. The evaluation of the vorticity field, ω_{xy}, for different grid resolutions, shows that the initial shear layer tickness was strongly affected by the coarser grid resolutions. In fact, a maximum grid spacing in the jet shear layer of $\Delta y = r_o/32$ was required for the accurate prediction of the jet flow dynamics. It was observed that the introduction of a near-inflow periodic excitation trigger the growth of Kelvin-Helmholtz instabilities, which rapidly evolve downstream to give rise to the vortex pairing process in the jet shear layer. The aerodynamic development of the vortex pairing proccess presents qualitative agreement with previous results taken from the literature at the same Reynolds number and inlet momentum thickness. The analysis of the corresponding acoustic field propagation shows that the dominant sound source produced in the jet shear layer was the sound radiated from the vortex pairing process, without any significant wave oscillations provided by the excitation. The particularly high directive character of sound radiation,

especially noticed at high Mach numbers, was attributed to the axisymmetric quadrupolar nature of the noise source. In the ongoing works, a parallel high-order finite-sized overlap flow solver is being developed to investigate Mach number and thermal instability effects arising from the heated three-dimensional round jets. It is hoped that high Reynolds number 3D computations of both cold and heated jet flow-noise sources and its inherently coupled noise propagation will allow us to investigate more deeply the underlying nonlinear mechanisms by which noise is aerodynamically generated in turbulent free shear layer flows at less idealized flow conditions.

6 ACKNOWLEDGEMENTS

This research project in computational aeroacoustics was supported by the LAE (Laboratory of Aerodynamics), Department of Aeronautical Engineering, University of São Paulo, Brazil. The project was sponsered by FAPESP (Fundação de Amparo à Pesquisa do Estado de São Paulo) which we gratefully thank for the financial support.

References

[1] Bodony, D. J. and Lele, S. K. On using large-eddy simulation for the prediction of noise from cold and heated turbulent jets. *Phys. Fluids*, 17:85–103, 2005.

[2] Boersma, B. J. and Lele, S. K. Large eddy simulation of Mach 0.9 compressible jet. *AIAA paper 99-1874*, 1999.

[3] Bogey, C. Calcul direct du bruit aérodynamique et validation de modèles acoustiques hybrides. Thesis, École Centrale de Lyon, Lyon - France, 2000.

[4] Bogey, C. and Bailly, C. LES of a high Reynolds, high subsonic jet : effects of the inflow conditions on flow and noise. In *AIAA, Paper No. 2003-3170*, 2003b.

[5] Bogey, C. and Bailly, C. LES of a high Reynolds, high subsonic jet : effects of the subgrid modellings on flow and noise. *AIAA, Paper No. 2003-3557*, 2003c.

[6] Bogey, C. and Bailly, C. Effects of inflow conditions and forcing on subsonic jet flows and noise. *AIAA J.*, 2005a.

[7] Bogey, C. and Bailly, C. Computation of a high Reynolds number jet and its radiated noise using large eddy simulation based on explicit filtering. *Computat. Fluids*, 33:1344–1358, 2006.

[8] Bogey, C. and Bailly, C. and Juvé, D. Noise investigation of a high subsonic, moderate Reynolds number jet using a compressible large eddy simulation. *Theor.Comput. Fluid Dyn.*, 16(4):273–297, 2003a.

[9] Bradshaw, P. The effect of initial conditions on the development of a free shear layer. *J. Fluid Mech.*, 1966.

[10] Choi, D. and Barber, T. J. and Chiappetta, L. M. Large eddy simulation of high-Reynolds number jet flows. *AIAA paper 99-0230*, 1999.

[11] Colonius, T. and Lele, S. K. and Moin P. Boundary condition for direct computation of aerodynamic sound generation. 1993.

[12] Colonius, T. and Lele, S. K. and Moin P. Sound generation in a mixing layer. *J. Fluid Mech.*, 330:375–409, 1997.

[13] Dimotakis, P. E. and Brown, G. L. The mixing layer at high reynolds number: Large-structure dynamics and entrainment. *J. Fluid Mech.*, 78:535–560, 1976.

[14] Freund, J. B. and Lele, S. K. and Moin, P. Numerical simulation of a Mach 1.92 turbulent jet and its sound field. *AIAA Journal*, 38(11):2023–2031, 2000.

[15] Gaitonde, D. V. and Visbal, M. R. High-order schemes for Navier-Stokes equations Algorithm and implementation into FDL3DI. *Technical Report AFRLVA-WP-TR-1998-3060, Air Force Research Laboratory, Wright-Patterson, AFB*, 1998.

[16] Gaitonde, D. V. and Visbal, M. R. Further development of a Navier-Stokes solution procedure based on higher-order formulas. *AIAA Paper No. 99-0557*, 1999.

[17] Galdi, G. P. In *Lectures in Mathematical Fluid Dynamics*. Birkhäuser-Verlag, Basel, Switzerland, 2000.

[18] Germano, M. and Piomelli, U. and Moin, P. A dynamic subgrid-scale eddy viscosity model. *Phys. Fluids A*, 3:1760–1765, 1991.

[19] Hill, Jr. W. and Jenkins, R. C. and Gilbert, B. L. Effects of the initial boundary-layer state on turbulent jet mixing. *AIAA J.*, 14:1513–1514, 1976.

[20] Islam, M. T. and Ali, M. A. T. Mean velocity and static pressure distributions of a circular jet. *AIAA J*, 35:196–197, 1997.

[21] Kim, J. and Choi, H. Large eddy simulation of a circular jet: effect of inflow conditions on the near field. *J. Fluid Mech.*, 620:383–411, 2009.

[22] Lele, S. K. Compact finite difference schemes with spectral like resolution. *J. Comput. Phys.*, 103:16–42, 1992.

[23] Leonard, A. Energy cascade in large eddy simulations of turbulent fluid flows. *Adv. Geophys*, 18A:237–248, 1974.

[24] Lilly, D. A proposed modication of germano subgrid-scale closure method. *Phys. Fluids*, 4:633–635, 1992.

[25] Mathews, J. and Lechner, R. and Foysi, H. and Sesterhenn, J. and Friedrich, R. An explicit filtering method for large eddy simulation of compressible flow. *Phys. Fluids*, 15(8):2279–2289, 2003.

[26] Michalke, A. On the inviscid instability of the hyperbolic-tangent velocity prole. *J. Fluid Mech.*, 19:543–566, 1964.

[27] Mitchell, B. E. and Lele, S. K. and Moin P. Direct computation of the sound generated by vortex pairing in an axisymmetric jet. *J. Fluid Mech.*, 383:113–114, 1999a.

[28] Moser, C. and Lamballais, E. and Gervais, Y. Direct computation of the sound generated by isothermal and non-isothermal mixing layers. *The 12th AIAA/CEAS Aeroacoustic conference, AIAA 2006-2447*, 2006.

[29] Park, N. and Lee, S. and Choi, H. A dynamic subgrid-scale eddy-viscosity model with a global model coefficient. *Phys. Fluids*, 18:125–129, 2006.

[30] Pascarelli, A. and Piomelli, U. and Candler, G. V. Multi-block large-eddy simulationsof turbulent boundary layers. *J. Comput. Phys.*, 257(256), 2000.

[31] Sagaut, P. Large eddy simulation for incompressible flows. *Springer Verlag*, 2001.

[32] Sesterhenn, J. A characteristic-type formulation of the Navier-Stokes equations for high order upwind schemes. *Comput. Fluids*, 30:37–67, 2001.

[33] Stolz, S. and Adams, N.A. An approximate deconvolution procedure for large eddy simulation. *Phys. Fluids A*, 11:1699–1701, 1999.

[34] Stolz, S. and Adams, N.A. and Kleiser, L. An approximate deconvolution model for large-eddy simulations of compressible flows and its application to shock-turbulent-boundary-layer interaction. *Phys. Fluids*, 13:2985–3001, 2001a.

[35] Tanna, H. K. An experimental study of jet noise. part i: Turbulent mixing noise. *J. Sound Vib.*, 50:405–428, 1977.

[36] Visbal, M. R. and Gaitonde, D. V. Very high-order spatially implicit schemes for computational acoustics on curvilinear meshes. *J. Comput. Acoust.*, 9(1):16–42, 2001.

[37] Vreman, A. W. An eddy-viscosity subgrid-scale model for turbulent shear flow: algebraic theory and applications. *Phys. Fluids A*, 16(10):3670–3681, 2004a.

[38] Yan, H. and Knight, D. Large-eddy simulation of supersonic at plate boundary layer part i. *AIAA Paper 2002-0132*, 2002.